Characterisation of mutatations in the *TTC7A* gene associated with Very Early Onset of Inflammatory Bowel Disease

Report

Major Research Project
MSc Regenerative Medicine & Technology

Polina Deenichina

Pediatric Gastroenterology Division of Regenerative Medical Centre Utrecht

Daily supervision:
Michal Mokry

First Examiner:
Edward Nieuwenhuis

Second Examiner:
Ewart Kuijk

UMC Utrecht

Utrecht University

Summary

The lining of our guts is made up of epithelial cells that create a barrier which prevents the spilling of intestinal contents into the rest of the body. Breakages in this epithelial barrier can lead to digestive problems and infection. Such barrier abnormalities accompanied with inflammation, often fatal, have been found in newborns and young children diagnosed with different diseases of the intestines and immune system. As a consequence, the gene *TTC7A* has been identified as a potential source for those abnormalities. The role of *TTC7A* in the maintenance of the epithelial barrier and in immune cells is not well-understood and therefore a cure does not exist. To address this gap in knowledge, we used small models of the gut, called organoids, taken from patients with *TTC7A* disease. Our organoids reflected the various epithelial defects observed in patients. We discovered novel interactions of TTC7A with other genes and their products responsible for cellular structure, and identified a drug that can help restore the function of the epithelial barrier. Our testing model can be used as a diagnostic tool to characterise epithelial abnormalities in patients and to test their responsiveness to a range of drugs.

Abstract

The tetratricopeptide repeat domain 7A (*TTC7A*) has been classified as a keeper of intestinal health for its vast functions in the gut epithelium, primarily in cytoskeletal organisation. The cytoskeleton is important for the correct polarisation of epithelial cells and therefore for maintaining the gut epithelial barrier, that separates the luminal contents from the entirety of the body, while supporting nutrient and waste transport. Cell polarisation, membrane identity and survival are highly dependent on phosphatidylinositol 4-kinase IIIa (PI4KIIIa), a specific binding partner of TTC7A. Loss-of-function of *TTC7A* or PI4KIIIa, can lead to gastrointestinal distention, necrosis, and mucosal destruction. The Rho pathway is another major regulator of the cytoskeleton that is thought to interact with TTC7A to maintain cell proliferation and survival. Recent efforts targeting the TTC7A pathway revealed the inhibition of Rho effectors (ROCK) corrected apicobasal polarity defects and Leflunomide increased cell survival in *TTC7A*-deficient models. In the last 5 years, more than 20 mutations have been identified in *TTC7A* associated with inflammatory bowel disease (IBD) characterised by variable disruptions to the gut epithelium and immunodeficiency. We have identified patients with epithelial phenotype carrying compound heterozygous *TTC7A* mutations who display heterogenous epithelial polarisation defects. Insufficient polarisation is considered the underlying cause for epithelial barrier disfunction, however, the genotype-phenotype correlation is still elusive and no effective treatment exists. In this paper, we sought to elucidate the role of *TTC7A* in pathological mechanisms associated with IBD by employing a model system of patient-derived *TTC7A*-deficient organoids. Immunostaining revealed that apicopasal polarity and morphology were corrected by ROCK inhibition, and not by Leflunomide. As there are numerous mutations within the TTC7A that may be associated with IBD, we investigated the individual effects of different mutations on a protein level. We generated a library of FLAG-tagged TTC7A mutant constructs that were transiently transfected into immortalised epithelial and hepatic cells. Immunoblotting revealed that 10 out of 11 transfected TTC7A mutations caused underexpression of their gene products. Immunoprecipitation and a competitive ELISA showed that missense TTC7A variants did not interrupt binding to PI4KIIIa and its enzymatic function.

Key words: inflammatory bowel disease ▪ intestinal organoids ▪ apicobasal polarity ▪ epithelial barrier ▪ TTC7A

Abbreviations

VEO-IBD – Very early onset of inflammatory bowel disease
MIA – Multiple intestinal atresia
CID – Combined immunodeficiency
EFR3 – Protein EFR3
HSC – Haematopoietic stem cell
PI4KIIIa – phosphatidyl-inositol 4-kinase III alpha
PI4P – phosphatidyl inositol 4 phosphate
PIP – phosphatidyl inositol-phosphate lipid
ROCK – p160-Rho-associated coiled-coil kinase
SD/THE = Syndromic Diarrhoea/Trichohepatoenteric Syndrome
TRP – tetratricopeptide repeat
TTC7A/B – tetratricopeptide repeat domain 7A/B

Introduction

Tetratricopeptide repeat domain 7A (*TTC7A*) is a conserved gene that has 2 splice isoforms, the most common consisting of 20 exons that code for 858 amino acids [1]. Although the crystal structure is still elusive, information from its paralogue Tetratricopeptide repeat domain 7B (TTC7B) with 49.47% sequence identity, revealed the presence of multiple tetratricopeptide (TRP) domains that are helix-turn-helix structurally conserved motifs, thought to play a role in protein scaffolding and multiple protein interactions [2–4]. *TTC7A* has 9 TRP domains that facilitate binding with Phosphatidylinositol 4-kinase III alpha (PI4KIIIa), FAM126, and EFR3, members of the conserved PI4KIIIa complex [5,6]. It has been demonstrated in yeast that TTC7A interacts with the PI4KIIIa complex independently from TTC7B, and has been recently identified a specific binding partner to PI4KIIIa [7–9]. PI4KIIIa phosphorylates phosphatidylinositol (PI) at the 4-potistion of the inositol ring to generate phosphatidylinositol-4-phosphate (PI4P) at the plasma membrane [10,11]. PI4P has been implicated in numerous cellular processes, and recently established as an important determinant of plasma membrane identity whereby synthesis and adequate distribution of PI4P is exclusively dependent on PI4KIIIa function and localisation [12–14]. In turn, TTC7A is necessary for the cycling of PI4KIIIa to the plasma membrane and thus indirectly regulating PI4P production and distribution [12,15,16]. There is strong evidence to support that PI homeostasis and PI4KIIIa are important for intestinal health [17,18]. Due to its interaction with multiple signalling pathways, *TTC7A* has been referred to as a steward of intestinal health by Jardine et al, playing a critical role in maintaining cytoskeletal structure, cell polarity, epithelial integrity, signalling homeostasis, and survival [20]. There is emerging evidence that TTC7A might have a regulatory function as a nuclear factor however, this is not in the scope of this report [21].

Recent advances in whole-exome sequencing have allowed the discovery of over 20 private *TTC7A*-disease carrying mutations in more than 50 patients, ranging from homozygous deletions to compound heterozygous missense mutations [22–26]. Although *TTC7A* RNA expression is comparable in many tissues, associated disruptions are presenting primarily in the gut and immune system [3,27]. *TTC7A*-related diseases are inherited as autosomal recessive and can cause symptoms with varying degrees of severity. Patients can experience from mild skin and hair-related features to severe disruptions in the epithelial gut lining and architecture that could lead to Very Early Onset of Inflammatory Bowel Disease (VEO-IBD), Multiple Intestinal Atresia (MIA), Apoptotic Enterocolitis (AP) and sometimes combined immunodeficiencies (CIDs) [22,24–26,28–39]. Immunosuppressive therapies, steroids, antibiotics, stem cell transplantations and intestinal resections are among the available options for patient care [25,28,40–43].Those treatments can alleviate some symptoms (e.g. haematopoietic stem cell transplantation is a viable option for CID) but have been proven ineffective in halting the progression of *TTC7A*-related diseases and in preventing lethality [28,40]. Providing adequate treatment is often challenging as the heterogenous disease presentation combined with multiple mutations, impedes correlation between phenotypical features and genetic makeup [44].

The main cause for *TTC7A* diseases is considered to be disrupted intestinal epithelium, signatures of which are disorganised pseudostratified cellular structures, low number of villi and increased apoptosis, in turn allowing pathogenic invasions from the gut into the immune system. A recent phenotypic high-throughput drug screen for reducing apoptosis without inducing uncontrolled cell proliferation, identified Leflunomide as a candidate drug for treating *TTC7A* deficiencies. Leflunomide increased cell viability in TTC7A-KO cells, rescued abnormal intestinal phenotype in *ttc7a*$^{-/-}$ zebrafish and enhanced survival of TTC7A-deficient patient-derived colonoids [45]. In the same study, small molecule inhibitors of p160-Rho-associated coiled-coil kinase (ROCK), an effector of the Rho signalling pathway, were compared to the effects of the candidate drug, as previous reports suggest that *TTC7A* phenotypes such as aberrant cell polarisation could be underlined by constitutive ROCK activation [29]. Bigorgne demonstrated that ROCK inhibitor Y-27632 was able to correct the polarity of inverted *TTC7A*-deficient patient-derived organoids. There is strong evidence to support that Rho signalling is essential for gut health and apicobasal polarity, and that it interacts with TTC7A, to maintain survival and proliferation. [46–50].

Knowledge on the *TTC7A*-caused pathogenesis in IBD is still lacking, primarily because linking the wide array of disease phenotypes to characterised *TTC7A* mutations, has been challenging. Our study aims to bridge this gap by investigating the effects of deficient *TTC7A* variants on epithelial polarisation and morphology, and on the TTC7A interactome. To do this, we used immortalised cell lines and intestinal organoids derived from healthy donours and *TTC7A*-deficient patients. We chose the organoid system as because it recapitulates the structure and function of the originating intestinal epithelium and furthermore reflects the genetic and epigenetic makeup of the patient, providing a route for developing peronalised treatments [51,52].

We successfully established duodenal-derived organoids as a robust system for *TTC7A* disease modelling. This emerging evidence on the effects of Leflunomide and ROCK inhibition on deficient *TTC7A*, prompt us to investigate further the efficacy of the drugs on organoid polarisation. ROCK inhibitor alone rescued inverted polarity defects in organoids derived from patients carrying compound heterozygous *TTC7A* mutations, whereas Leflunomide did not. Therefore, we identified ROCK inhibitor as a promising candidate for treating patients with an inverted epithelial phenotype. In an attempt to link genotype to phenotype, we generated a library of missense *TTC7A* mutations that were transiently expressed into immortalised epithelial and kidney-derived cell lines. Immunoblotting revealed that *TTC7A* mutant gene products were underexpressed with the exception of one variant. To gain a better insight into the mechanism behind polarisation, we immunoprecipitated mutant TTC7A and its binding partner PI4KIIIa. We were the first to report that herein studied mutant TTC7A variants did not interrupt interaction with PI4KIIIa. We then used a competitive ELISA to test the enzymatic activity of PI4KIIIa complexed with deficient TTC7A. The immunosorbent assay revealed that PI4KIIIa produced almost diminished levels of PI4P when TTC7A is mutated.

Materials and Methods

Cell/tissue cultures

Cell cultures

Commercially obtained HEK932T cells were passaged every 2 to 4 days and refreshed with Dublecco's Modified Eagle Media (DMEM) enriched with high glucose, GlutaMAX and pyruvate (31966021, Gibco) supplied with 10% Foetal Bovine Serum (FBS) and 50 U/mL Penicillin/Streptomycin (P/S) (15140-122, Gibco). Caco2BBe (C2BBe) are a gift from Jerold Turner, Boston, and *TTC7A* was knocked out by CRISPR/Cas in our lab. C2BBe TTC7A-KO cells were passed every 2 to 7 days and refreshed with DMEM, high glucose (41965039, Gibco) supplied with 10% FBS, 50 U/mL P/S (15070063, Gibco) and 0.085 M HEPES (15630080, Gibco). For passaging, cells were washed with Phosphate-Buffered Saline 0 (PBS0 without Ca^{2+} and Mg^{2+}) and detached with prewarmed 0.05% Trypsin-EDTA (15400-054, Invitrogen). Trypsin was deactivated with prewarmed media, cells were seeded in ratios of 1-6 and all cell cultures were maintained in a 37°C, 5% $C0_2$ incubator.

Patient data

As a part of the VEOIBD consortium, our lab has generated the largest biobank for VEO-IBD patients. VEO67 biopsy hereby referred to as Patient 1 from ileum (P1 ile) and STE165 biopsy hereby referred to as Patient 2 from duodenum (P2 duo) were obtained via a distal ileostomy and proximal ileostomy, and via a flexible gastroduodenoscopy, respectively, performed as standard diagnostic procedures. P1, 18 years, was diagnosed with UC and has a compound heterozygous mutation in the 2086T>C and 1817A>G coding regions of *TTC7A*, as well as in the coding region 2224C>A of its paralogue *TTC7B*. P2, 13 years, was diagnosed with immunodeficiency and enteropathy and has a compound heterozygous mutation in the 518G>T and 1355T>C coding regions of *TTC7A*. For control organoids lines, healthy donour biopsies expressing wild type *TTC7A* were obtained from ileum and duodenum by ileo-colonoscopies and gastroscopies as a part of standard diagnostic procedures. Three control organoid lines for each patient were grown from the biopsies, ileum 1, 2 and 3 (ile 1-3) for P1 and duodenum 1, 2 and 3 (duo 1-3) for P2. Human material used in this study was approved by the Ethics Committee Boston's Children Hospital, by the Ethics Committee (Medisch Ethische Toetsings Commissie, METC) and University Medical Centre Utrecht.

Organoid cultures

Isolation of intestinal crypts was executed as previously described [50]. Isolated crypts were embedded in 50-70% matrigel (356231, Corning) and growth factor-free medium (GF-) consisting of DMEM/H2 (010, Gibco), P/S 50 U/mL (15070063, Gibco), 0.05 M HEPES (15630080, Gibco) and 1% Glutamax (15630-056, Gibco). Three times a week, organoids were refreshed with human Small Intestinal Expansion Medium (hSI-EM) enriched with 50% Wnt, 20% R-spondin, 10% Noggin, 0.005 ng/mL mEGF, 0.01 M Nicotinamide, 0.125 M N-acetyl, 1x B27, 0.05 µM TGF-b inhibitor (A83-01), 10 µM P38 inhibitor (SB2021190), Primocin 100 µg/ml. All ileum lines were supplied with hSI-EM containing 25% R-spondin, instead of 20%. For maintenance, organoids were passaged approximately every 3 to 10 days, by mechanical dissociation in a ratio between 1:1 and 1:4, or by single cells using TrypleE (1:1000, 12604021, ThermoFisher Scientific). For both passaging methods, matrigel was dissolved using prechilled GF- and organoids were collected and centrifuged at 1600 RPM for 5' at 4°C, after which supernatant was aspirated. For mechanical dissociation, organoids were resuspended repeatedly using a p200 tip inserted into a p1000 pipette tip in cold GF-. This was followed by centrifugation using the same settings, supernatant was removed and organoid fragments were plated in

prewarmed 24-well plates in 2-4 droplets of 10-25 μL 50-70% Matrigel x GF-. For single cell passaging, TrypleE was added and incubated for 5 to 10' at 37°C. Organoids were resuspended vigorously until single cells were visible under a stereomicroscope. TripleE was inactivated with GF- and the cell suspension was centrifuged with the same settings. Cells per well were seeded in matrigel droplets described above. Single cell cultures are refreshed with hSI-EM supplemented with 10 uM ROCK inhibitor (Y-27632, 120129, Abcam) for 2-3 days, after which only hIS-EM was used. All cultures were kept at 37°C, 5% $C0_2$ incubator. Morphology and overall condition of organoids was monitored using EVOS cell imaging system (ThermoFisher Scientific).

Apicobasal polarity

Sample preparation

Apicobasal polarity assay was carried out in 96-well clear flat bottom imaging plates. Following mechanical dissociation, ~200 organoid fragments were seeded in 7.5 μL droplets of 1:1 matrigel:GF- per well. Organoids were supplied with hSI-EM in the presence or absence of Leflunomide (PHR1378-1G, Sigma-Aldrich chemie), Y-27632, or both, to a final concentration of 10 μM each dissolved in DMSO, for 3-4 days. On the final day, organoids were washed with PBS and fixed in cold 4% paraformaldehyde for a minimum of 1h. Following fixation, organoids were permeabilised with permeabilization buffer (PB) 0.3% Triton X100 x PBS for 30' at 4°C, or alternatively were stored in PBS wrapped in parafilm at 4°C for up to a week. Subsequently, PB was substituted with 5% blocking buffer (BB) containing Bovine Serum Albumin (BSA) dissolved in PB, for 1h.

Immunofluorescent imaging and data analysis

Primary antibodies rat-anti-human DC49F binding a6-integrin (1:250, 555734, BD Biosciences) and purified rat IgG2 isotype control (1:250, 555841, BD Biosciences) were dissolved in BB overnight (o/n) at 4°C. The following day, antibody mixes were removed, and wells were washed 3 times with PB for 5' at RT on a plate shaker. TRITC-labelled phalloidin (1:100, P1951, Sigma) that binds F-actin and secondary antibody Goat-anti-Rat-IgG-(H+L)-Alexa 647-conjugate A094 (1:800, A21247, ThermoFisher) were dissolved in BB and incubated for 1h at RT in the dark. Following secondary staining, samples were washed 3 times with PB for 5' at RT on a plate shaker and the nuclei were stained with DAPI (2 mg/mL) for 15' at RT in the dark. Organoids were washed 3 times with PB for 5' at RT on a plate shaker. Then 100 μL of PBS per well were added and immediately imaged and/or stored in the fridge wrapped in parafilm and aluminium foil. Images were obtained with a 20X objective on a Confocal Leica SPX8 microscope and the LAS X Software. Imaging was performed well by well, as the Z-plane had to be manually adjusted per well to have a maximum number of organoids in focus. The excitation and emission spectra for DAPI were 405 nm and 410-521 nm, for Alexa Fluor 647 653 nm and 658-776 nm, for TRITC 551 nm and 565-635 nm, respectively. Laser intensities had to be adjusted for each experiment. Images were analysed with the Cell Counter function of ImageJ, whereby normal, inverted, and aberrant organoids were assigned by eye.

Site-directed mutagenesis

Vectors

Human *TTC7A* (Myc-DDK-tagged) pCMV6-TTC7A-myc-FLAG (RC217177, OriGene) with kanamycin antibiotic resistance was used as a template for creating *TTC7A* point mutations and for FLAG-tagged TTC7A protein detection. Vector pEGFP-C3 (V012022, Clontech), kanamycin resistant, was used as a quality control for cell transfection and a negative control for protein detection in western blot.

Primer design

Primers (Integrated DNA Technologies) were designed in overlapping sets of two (forward and reverse) for each mutation, following the QuickChange protocol, to specifically induce mutations that have been found to occur in the *TTC7A* gene reported in literature. A full list of primers used in this research can be seen in Table 1. Upon arrival the primers were diluted with sterile water to 100 μM and were preliminary tested with the *TTC7A* wild type template in a polymerase chain reaction (PCR) with temperature degrees increasing in increments using the Pfu Ultra High-Fidelity (Agilent) kit. This was done to establish the temperature at which the primers were most efficient. Then the PCR products were separated by size on a 1% electrophoresis agarose gel to confirm the presence or absence of the desired construct size as well as formation of primer dimers.

DNA amplification

Successful sets of forward and reverse primers per mutation were then used to create point mutations in *TTC7A* following the Pfu Ultra High-Fidelity (Agilent) manual. The settings of the thermocycler were determined by the size of the construct. Each PCR product was run on a 1% agarose gel to confirm if the reaction was successful. The leftover PCR products were digested with DpnI for 1h at 37°C. Following enzymatic treatment, the fragments could be stored

long-term at -20°C and/or be used for transformation of competent cells.

Molecular cloning

Transformation was carried out in Stellar competent cells following manufacturers protocol (Clontech, PT5055-2). For the kanamycin resistant vector, kanamycin (25 μg/mL) dishes were used. After o/n bacterial growth on the plates, individual colonies were collected in LB broth supplied with kanamycin and grown o/n at 37°C on a shaker (225-250 rpm). The following day, plasmid DNA was extracted from the o/n bacterial cultures following Invitrogen's PureLink Quick Plasmid Miniprep (K210011) protocol. 500 μL of each bacterial culture was stored in 4°C for a later use. Concentration and quality of the eluted DNA were measured on a nanodrop.

Analytical sequencing

To check whether the point-mutation was successfully created in the *TTC7A* gene, each miniprepped sample is sent to Macrogen to be sequenced. For each sample between 1 and 4 sequencing mixes are prepared to accommodate the different primers used pCMV6 Forward, TTC7A Begin, TTC7A Middle, TTC7A End (Table 1), which are determined by the location of the mutation on the gene. Sequencing results are then analysed in Benchling by aligning the samples to the corresponding vector containing the WT *TTC7A*.

Re-transformation

Confirmed mutants were expanded from previous mini DNA extraction leftovers, in larger quantities for a Maxi (12162, Plasmid Maxi Kit, Qiagen) DNA extraction following manufacturer's instructions. Prior to Maxi DNA extraction, 500 μL of each bacterial culture were mixed with 500 μL 50% Glycerol and stored at -80°C. Glycerol stocks are only prepared after sequencing confirmation of successful point mutants. Following the Maxi-prep procedure, concentration and quality of the eluted DNA were measured on a nanodrop. Each sample was diluted to 1000 ng/μL with sterile water and stored at -20°C.

Protein assays

Cell transfection

Following trypsinisation HEK932T and C2BBe TTC7A-KO cells were seeded in ratios of 1-4 in 6-well plates. At ~80% confluency, cells were transfected with WT (positive control) and mutant variants of *TTC7A* carried by the pCMV6-TTC7A-myc-FLAG vector following Invitrogen's Lipofectamine 3000 protocol using the minimum amounts of the suggested reagent quantities. One well was transfected with pEGFP-C3 for quality control of transfection. Cells were collected for sample preparation for a western blot or for coimmunoprecipitation 48h post-transfection.

Western blot sample preparation

Western blotting was used to establish TTC7A mutant protein expression compared to WT TTC7A levels. Previously transfected cells were washed with PBS0 and detached with prewarmed 0.05% Trypsin. Trypsin was deactivated with prewarmed appropriate cell media and transferred to 1.5 ml Eppendorf tubes. Cells were centrifuged at 4°C 1500 rpm for 5', washed with PBS0, vortexed and these steps were repeated. Lammeli Lysis Buffer (LLB) made up of 8% SDS, 5% Glycerol, 25 mM Tris-HCL pH 6.8, protease inhibitor tablets (1 per 25 mL) and demi water, added directly to the cells and the solution was resuspended immediately to avoid clumping. More LLB was added until the sample could be pipetted without difficulty. Protein concentration was measured following the ThermoFisher BCA kit protocol. Lysates were stored at -80°C and/or used for a western blot. Based on the BCA results, samples were diluted with LLB to 25 μg up to 45 μL, to which 2.48 μL of 20x Sample Buffer (20xSB) was added. 20xSB is made up of LLB, 0.1% Bromophenol Blue Salt, 14.2 M 2-Mercaptoethanol, and sterile water.

Co-immunoprecipitation sample preparation

The purpose of this assay was to confirm whether mutant TTC7A variants can directly bind PI4KIIIa. Adapted from [28], the coimmunoprecipitation protocol was optimised and established in our lab. To avoid protein-protein link dissociation all steps were performed as much as possible on ice and buffers were prechilled. Previously transfected cells were washed twice with ~3 mL of PBS0 and 500 μL of Avitzur Lysis Buffer (ALB) was added directly on top. ALB is made up of 150 mM NaCl, 50 mM HEPES, 1% TritonX100, 10% Glycerol, 1.5 mg $MgCl_2$, 1 mM EGTA and demi water. The lysates were scraped and centrifuged at max speed for 10-20' at 4°C. 15 μL of the lysate supernatant was mixed with 15 μL of 2x Sample Buffer (2xSB) and stored at -80°C – this served as a loading control/input for the coimmunoprecipitation blots. The remaining of the lysate supernatants were mixed with preequilibrated 20 μL of packed gel anti-FLAG M2 magnetic beads (Sigma Aldrich) per sample, following manufacturer's steps. The beads were incubated with the lysates with agitation at 4°C for 4h. Following precipitation,

the bead-protein complexes were washed with TBS buffer according to the bead manual, mixed with a protein stability buffer (TE) and 30-40 μL of 2xSB and stored at -80°C. 2xSB is made up of 125 mM Tris-HCL, pH 6.8, 4% SDS, 0.01% Bromophenol Blue Salt, 50 mM DTT, 25% Glycerol and demi water.

SDS-PAGE

Samples were vortexed, denatured at 95°C for 5' and immediately loaded on an 8% polyacrylamide SDS-PAGE gel to be separated by molecular mass. Gels were run at 100-150 V until the dye front reaches the bottom of the gel. The proteins from the gel were transferred to a polyvinylidene fluoride (PVDF) (Pierce) membrane following the 'wet transfer' method at ~30 V o/n at 4°C.

Antibody incubation

The membranes were blocked in 5% blocking solution consisting of Elk x Tris-buffered Saline with Tween 20 (TBST) for 1h at RT with agitation. Blocking solution was substituted with primary antibody mixes. Primary antibodies were each diluted in 0.5% Elk x TBST: human/mouse FLAG-TTC7A (F3165, SIGMA) and b-actin (47778, Santa Cruz) at 1:2000 in and 1:5000, respectively, with incubation time of 30', and rabbit anti-PI4KA (PA5-28570, ThermoFisher) and rabbit anti-cofilin (5175, Cell Signalling) were both diluted at 1:1000, with incubation time of 1h. Following primary antibody incubation, blots were washed with TBST four times, 5' each, with agitation. After washing, secondary antibody incubation followed. Secondary antibody mixes were prepared the same as primary using horseradish peroxidase (HRP)-conjugated swine-anti-rabbit or rabbit-anti-mouse (Invitrogen) antibodies at a concentration of 1:5000. All antibody incubations were carried out with agitation. After secondary incubation, blots were washed as previously with TBST and stored in PBS at 4°C and/or imaged.

Imaging and data analysis

The HRP enzyme serves as a substrate for a chemiluminescent reaction where signal is produced in the form of light and corresponds to protein concentrations on the blot. Blots were developed using various detection kits (Thermofisher's SuperSignal West Pico, West Femto Maximum Sensitivity Substrate, West Dura Extended Duration Substrate) depending on the band signal intensity. Signal was measured in a ChemiDoc Touch Imaging System (Bio-Rad) and settings were adjusted according to the protein signal intensity and to avoid overexposure. To calculate protein concentrations, signal from protein bands was scored by using the volume tools to subtract local background in the Image Lab software (Bio-Rad). Values of protein samples were normalised to the expression of the loading controls b-actin or cofilin.

Results

Morphological and apicobasal polarity analysis in healthy and *TTC7A*-deficient organoids

We investigated the morphological and apicobasal polarity of two patient-derived lines: Patient 1 ileum (P1 ile) and Patient 2 duodenum (P2 duo). As patient organoid lines were obtained from dissimilar intestinal locations, they each required unaffected controls to be isolated from the same intestinal locations. For P1 we used ileal 1, 2 and 3 and for P2 we used duodenal 1, 2 and 3 controls from healthy individuals.

Morphological phenotype in healthy and TTC7A-deficient intestinal organoids

First, we analysed the morphology in both ileum and duodenum lines for three parameters: circular or swollen organoids were considered normal and classified as 'cystic', deformed non-cystic and unable to structurally support their own weight were deemed 'collapsed', darkened aggregations of organoid tissue where distincs shapes could not be identified were assigned an 'aggregated' phenotype. Healthy ile 1 formed crypt-resembling exclusions away from the organoid lumen that is known as budding (Figure 1A) and were more collapsed than the other control lines ile 2 and ile 3 (Figure 1B). In contrast, ile 2 and 3 showed a more cystic phenotype, but with a slower growth and fewer organoids (Figure 1A and B). Ile 3, especially, was challenging to maintain in culture as its requirements were unpredictable and showed a considerable number of aggregations and deformities, compared to the other ileum controls (Figure 1B).

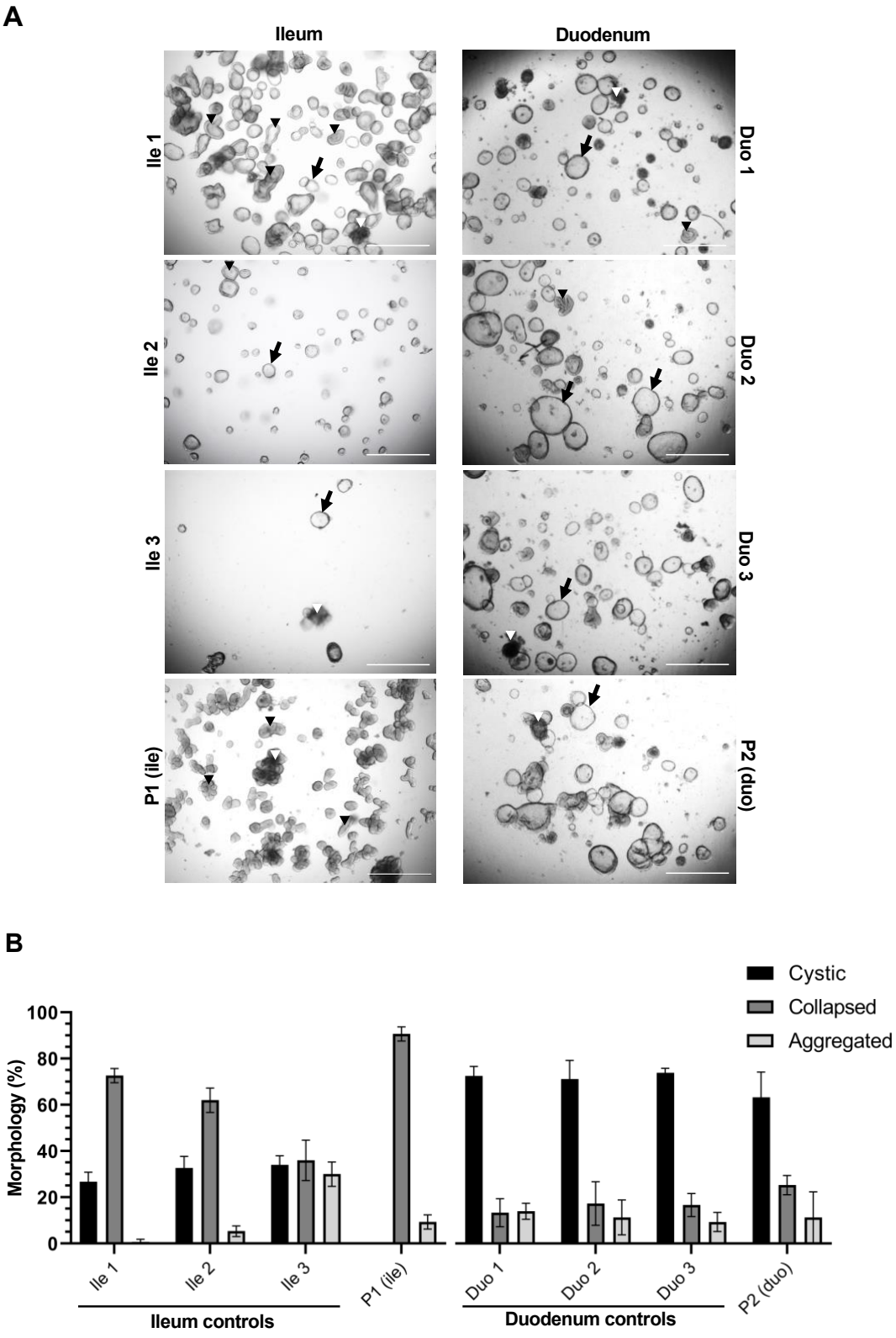

Figure 1. Morphological phenotype and quantification of intestinal organoids in hSI-EM

(A) Organoids were seeded by mechanical shearing and overall organoid condition was assessed for cystic (black arrow), collapsed (black arrowhead) and aggregation (white arrowhead) signatures. P1 (ile) and P2 (duo) represent *TTC7A*-deficient patient-derived organoids from ileum and duodenum, respectively. Ile 1-3 (ileum) and Duo 1-3 (duodenum) are healthy control lines for P1 (ile) and P2 (duo), respectively. Representative images were obtained with a stereomicroscope (EVOS) at a magnification of 4x and scale bar 500 μm.

(B) Morphology was quantified by counting 50 organoids per field (N=3) whereby cystic, collapsed or aggregated morphologies were assigned. Graphs were generated in GraphPad, error bars represent standard deviation.

In comparison to the ileum control lines, P1 (ile) had a faster growth rate established during routine passaging regiment and showed similar crypt-forming features and overall morphology to its control ile 1, however, consistently forming cell aggregations rather than being able to bud off (Figure 1A). P1 did not form cystic organoids and a clear lumen could not be observed.

Apicobasal polarity in healthy and TTC7A-deficient intestinal organoids

Organoids were analysed for the distribution of two polarity markers and were classified as 'normal' where F-actin is lining the lumen and a6-integrin is marking the apicobasal membrane, 'aberrant' where the polarity proteins have irregular patterns or there

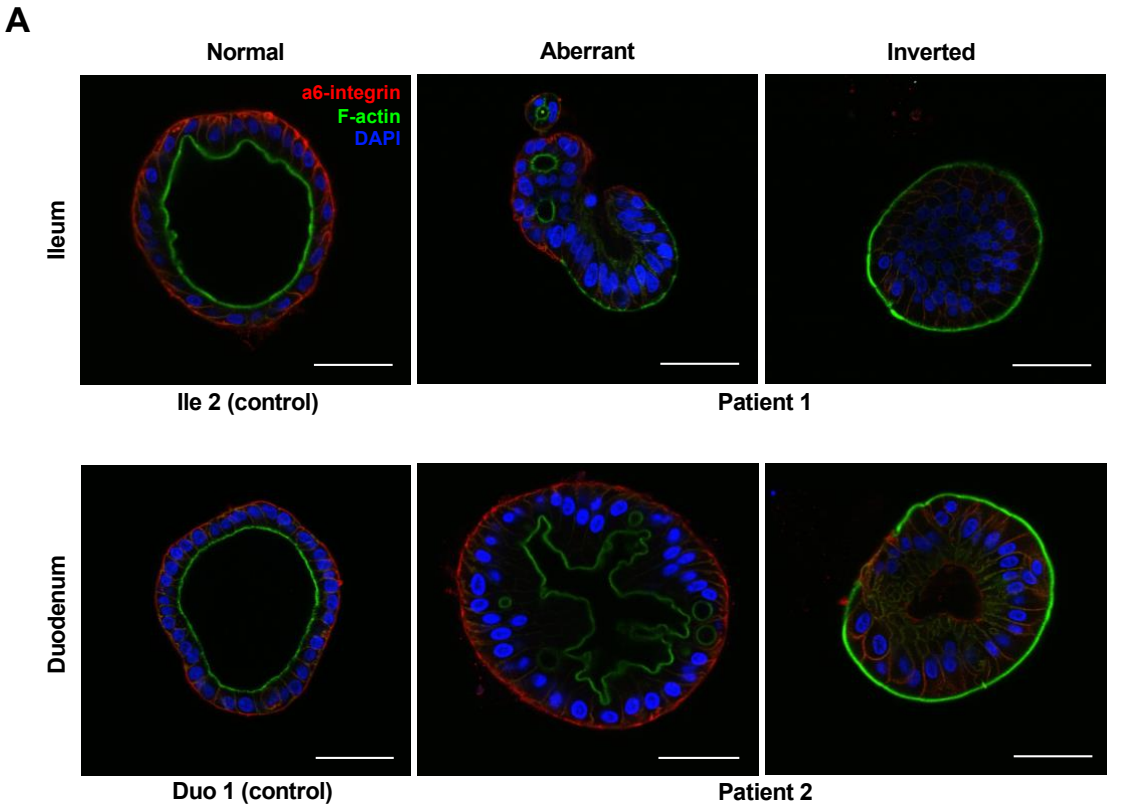

Figure 2. Apicobasal polarity quantification of intestinal organoids in hSI-EM

(A) Confocal images of organoids were obtained from Rinske Sparius and are representative of normal, aberrant, and inverted apicobasal polarity in ileal control 1 (ile 2) and *TTC7A*-deficient (Patient 1), and duodenal control (duo 2) and *TTC7A*-deficient (Patient 2) organoids. Prior to imaging organoids were sheared mechanically and then immunofluorescently labelled for polarity a6-integrin (red), F-actin (green), and nuclear DAPI (blue) markers. Magnification is 63x and scale bar is 50 μm.

(B) All organoid lines were maintained by single cell passaging prior to apicobasal experiment, then were mechanically dissociated, and seeded in 4-8 wells of 100-200 organoids per well. Then organoids were immunofluorescently labelled for a6-integrin, F-actin and DAPI and imaged with a confocal microscope. Apicobasal polarity in normal conditions (hIS-EM) was quantified in ImageJ as normal, aberrant, and inverted in healthy control lines of ileum (ile 1-3) and duodenum (duo 1-

3) for the respective P1 (ile) and P2 (duo) *TTC7A*-deficient patient-derived organoids. Graphs were generated in GraphPad, error bars represent standard deviation.

are multiple lamina formations instead of one, and 'inverted' where the F-actin and a6-integrin are completely swapped (Figure 2A).

It has been observed that healthy organoids can be inverted or aberrant during standard culturing regiments. Therefore, it is important to establish the baseline of normal apicobasal polarity in healthy controls. Ileum healthy lines scored an average of 72% normal apicobasal polarity from a single experiment (Figure 2B, Ileum). On the other hand, duodenum healthy controls from five experiments, produced a robust average of 83% for normal polarity in unaffected organoids (Figure 2B, Duodenum). Based on the established normal values for polarity, the abnormalities were assessed. P1 (ile) had no aberrant organoids and less inverted organoids compared to its ileum controls (Figure 2B, Ileum). Duodenum P2 showed a decrease in normality by ~20% compared to the average normal value of ~83% (Figure 2B, Duodenum). Within the P2 (duo), the aberrant and inverted together make up ~35%, of which approximately 2/3 are inverted and 1/3 are aberrant (Figure 2B, Duodenum).

ROCK inhibitor has a stronger correcting effect on inverted apicobasal polarity compared to Leflunomide in TTC7A-deficient duodenum organoids

To test the effects on apicobasal polarity defects, we treated all duodenum lines with Leflunomide, ROCK Inhibitor (Y-27632), or both. Untreated *TTC7A*-deficient organoids had a ~20% decrease in normality compared to healthy controls (Figure 3A), as previously shown (Figure 2B, Duodenum). The addition of Y-27632 returned normality of P2 organoids to homeostatic levels, but Leflunomide did not. The combination of both drugs together returned polarity to normal. ROCK inhibitor corrected invertedness but had no effect on aberrant luminae formation. Similar results were observed using the drugs in combination.

ROCK inhibitor improves morphology and rescues the inverted defect in TTC7A-deficient patient-derived duodenum organoids

We further examined the effect of ROCK inhibitor on polarisation on defects and correlated it to morphological signatures of normal or aberrant organoids. Under expansion media (hSI-EM), P2 had significantly less normal organoid polarity compared to healthy controls (Figure 3B). Patient organoids treated with ROCK inhibitor showed a significant increase in normality compared to untreated *TTC7A* mutants, and superseded untreated healthy controls (Figure 3B). Confirming previous observation (Figure 3A), ROCK inhibitor rescued the inverted phenotype but did not have an effect on multiple lumina formation. Moreover, Y-27632 decreased significantly the collapse of organoid structures and clustered aggregations in both healthy controls and patient lines (Figure 3C and D).

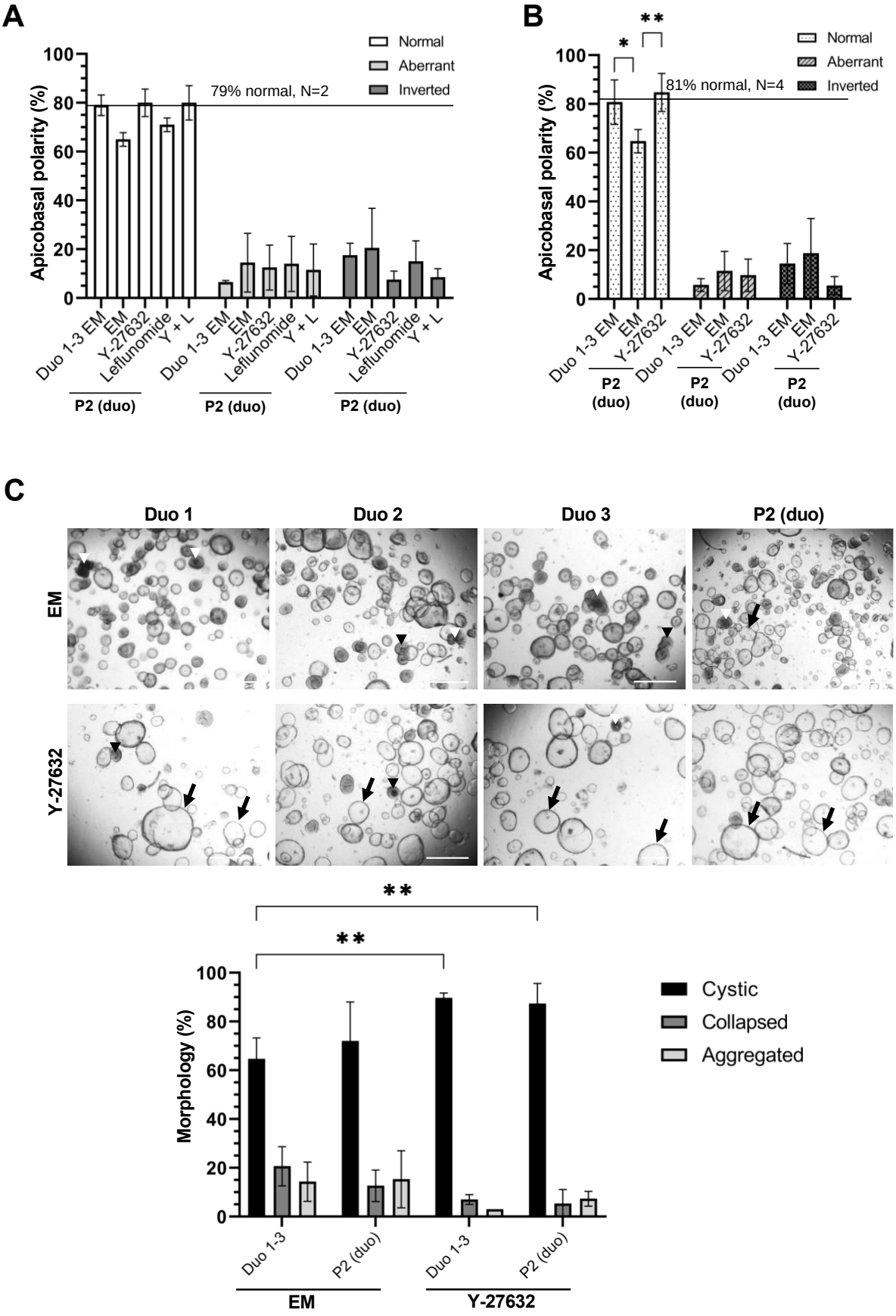

Figure 3. Apicobasal polarity and morphology quantification of duodenal organoids treated with Leflunomide, ROCK inhibitor or combined.

(A) All organoid lines were maintained by single cell passaging prior to apicobasal experiments, then were seeded in 4-8 wells of 100-200 organoids per well by mechanical shearing and were treated without (his-EM) or with Leflunomide, ROCK inhibitor (Y-27632) or both (Y + L), N=2.

(B) The above-described experiment was replicated only with the addition of ROCK inhibitor (Y-27632), N=4. Healthy duodenum controls are represented by Duo 1-3 and Patient 2 is represented by P2 (duo). Following immunofluorescent staining,

organoids were assigned normal, aberrant, or inverted polarity by eye according to the distribution of a6-integrin and F-actin using a confocal microscope and ImageJ.

(C) Morphological comparison between treated (Y-27632) and untreated (EM) duodenum organoids was assigned as cystic, collapsed, or aggregated by counting 50 organoids per field (N=3) in ImageJ. Representative images were obtained with a stereomicroscope with 4x magnification, scale bar is 500 μm. Values were normalised to the total number of organoids for each group and averages of each experiment were used to perform 2-way ANOVA statistical analyses in GraphPad (p > 0.05 - ns; p </= 0.05 - *; p </= 0.01 - **; p </= 0.001 - ***; p </= 0.0001 - ****). Error bars represent standard deviation.

Deficient TTC7A protein expression and interaction with PI4KIIIa

TTC7A KO has no effect on epithelial cell morphology

We did not find any difference in morphology or phenotypic features of apoptosis such as blebbing between C2BBe WT and C2BBe TTC7A-KO cells (Figure 4A), and western blot confirmed the TTC7A knockout (Figure 4B). The only observed dissimilarity was that the knockout cells required less frequent passaging.

Transient expression of deficient TTC7A gene products in epithelial cells

FLAG-tagged *TTC7A* single point mutations (Table 1) were transiently expressed each in epithelial cells knocked out of *TTC7A* (C2BBe TTC7A-KO) and their individual effects on gene products were analysed. All mutations resulted in underexpression of TTC7A compared to WT TTC7A, except for S539L TTC7A, which was overexpressed by ~10% (Figure 4C).

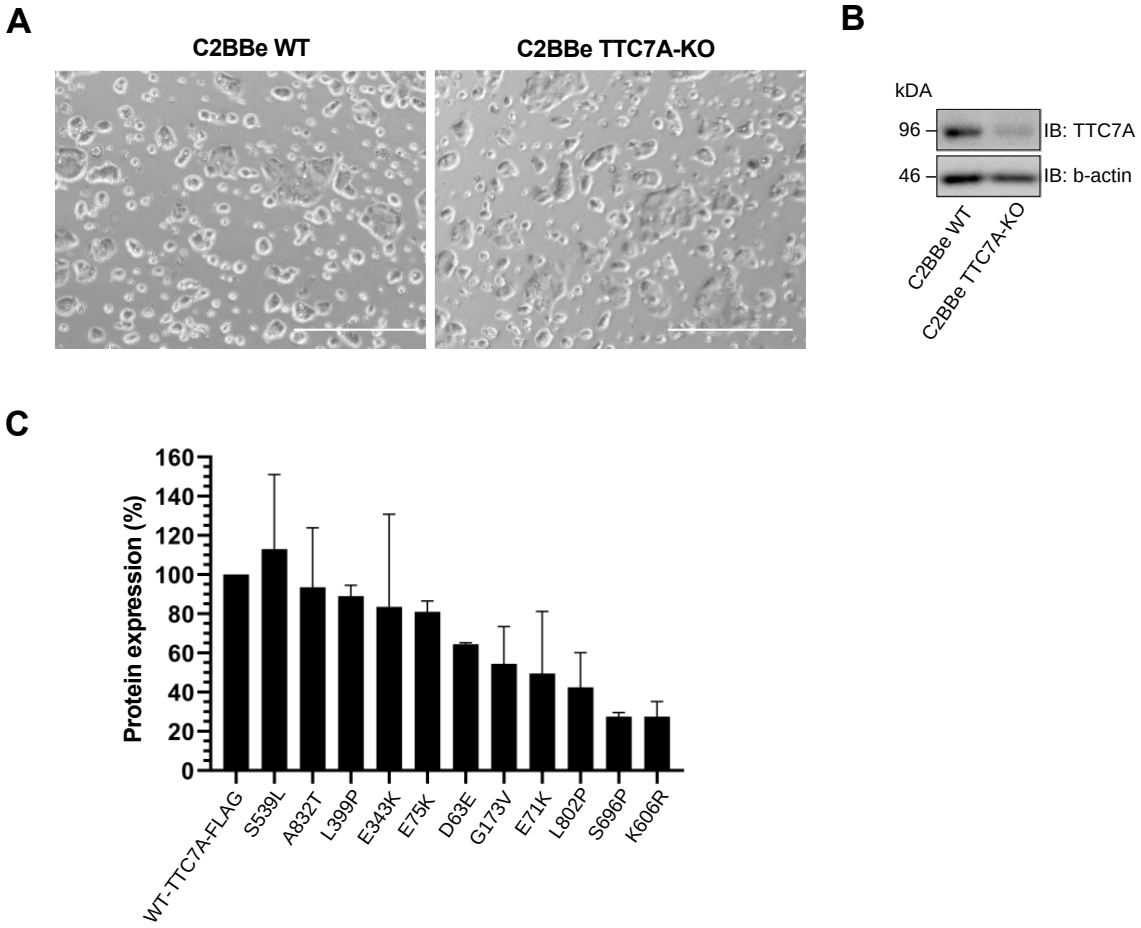

Figure 4. Morphology and protein expression in C2BBe WT and C2BBe TTC7A-KO cells.

(A) Confluent C2BBe WT and C2BBe TTC7A-KO cells were passaged in a ratio of 1:3 and imaged with a bright field stereomicroscope at 10x magnification. Scale bars are 500 μm.

(B) (B) C2BBe WT and C2BBe TTC7A-KO cells were lysed and immunoblotted with anti-TTC7A and anti-b-actin. TTC7A protein expression values were normalised to the b-actin loading control.

(C) C2BBe TTC7A-KO cells were transiently transfected with FLAG-tagged WT or missense TTC7A variants which are annotated with the corresponding amino acid substitution code. Protein expression values were normalised to b-actin and then to WT TTC7A-FLAG in ImageLab Graph was produced in GraphPad and error bars represent standard deviation.

TTC7A mutation	Site-directed mutagenesis forward and reverse primers	Affected tissue and diagnosis
c. 189C>G p. **D63E**	CTTTCCGGACACCGATGAGTTTGGGAAATTGCTGCTG CAGCAGCAATTTCCCAAACTCATCGGTGTCCGGAAAG	Duodenum, jejunum, ileum; IBD-MIA-CID [32]
c. 211G>A p. **E71K**	GAAATTGCTGCTGGCTAAGGCCCTCCTGGAGC GCTCCAGGAGGGCCTTAGCCAGCAGCAATTTC	Pylorus, duodenum, ileum, colon; IBD-MIA-CID [28–30]
c. 223G>A p. **E75K**	GGCTGAGGCCCTCCTGAAGCAGTGTTTGAAGG CCTTCAAACACTGCTTCAGGAGGGCCTCAGCC	Ileum, colon; IBD-CID [52]
c. 518G>T p. **G173V**	GCTTTTGTCATCAAAGTCCTCTCTCTGGAACG CGTTCCAGAGAGAGGACTTTGATGACAAAAGC	Duodenum, colon; polarity disorders; present in Patient 2 (unpublished)
c. 1027G>A p. **E343K**	CAAGGACAACATCAAGGAAGCCCTCCTGC GCAGGAGGGCTTCCTTGATGTTGTCCTTG	Colon; normal morphology (unpublished)
c. 1355T>C p. **L452P**	GACCCCACCGTGCCCCCGATGGCCGCGAAGGTC GACCTTCGCGGCCATCGGGGGCACGGTGGGGTC	Duodenum, colon; polarity disorders; present in Patient 2
c. 1576C>T p. **Q526X**	GAGAGGGCTCAGTAGCTGGCGCCCAG CTGGGCGCCAGCTACTGAGCCCTCTC	Duodenum, colon; IBD-CID [28,53]
c. 1616C>A p. **S539L**	CCAGGTCATCCTCTATGTCTTGCTGCAGCTGGCCCTCGTC GACGAGGGCCAGCTGCAGCAAGACATAGAGGATGACCTGG	Ileum, colon; IBD-SD/THE [31,47]
c. 1817A>G p. **K606R**	CAACCTGATGTTCACCAGGGTGAAGCTGGAGCAGG CCTGCTCCAGCTTCACCCTGGTGAACATCAGGTTG	Ileum; cystic fibrosis morphology; present in Patient 1 (unpublished)
c. 2086T>C p. **S696P**	CTGACTATGCCCCCTTCGGTCCTGAAG CTTCAGGACCGAAGGGGGCATAGTCAG	Ileum; cystic fibrosis morphology; present in Patient 1 (unpublished)
c. 2405T>C p. **L802P**	GAGCTTGGCCCAGAAGGTGCCTCGTGATGCCGTGGAGAGGC GCCTCTCCACGGCATCACGAGGCACCTTCTGGGCCAAGCTC	Colon; normal morphology (unpublished)
c. 2494G>A p. **A832T**	CCAGGGCCAGAACGAGGCTAGTTGACTG CAGTCAACGGTAGCCTCGTTCTGGCCCTGG	Cecum; IBD [28] polarity disorders (unpublished)

Analytical sequencing forward primers	
pCMV6	CGCAAATGGGCGGTAGGCGTG
TTC7A Begin	GGAAGCTGCCCTCCAGAGCGCC
TTC7A Middle	GGCCCTCGTCCGACAGATCTCC
TTC7A End	CCCAGATGGCGTGCGCATC

Table 1. *TTC7A* site-directed mutagenesis primers and patient-derived data
c. = codon, ch. = chromosome, CID = Chronic Intestinal Dysmotility, IBD = Inflammatory Bowel Disease, MIA = Multiple Intestinal Atresia, p. = protein, SD/THE = Syndromic Diarrhoea/Trichohepatoenteric Syndrome. Primer orientation is 5' → 3'.

HEK293T cell line is a more reliable model for transient transfection and exogenous protein expression

We transfected C2BBe TTC7A-KO and HEK293T cells with fluorescent-expressing pEGFP-C3 to visualise transfection, and with pCMV6-TTC7A-WT-FLAG to compare exogenous protein expression. Evidently, the epithelial cells display a very low transfectability even after 48h, compared to HEK293T cells at 24h (Figure 5A). Transfected with pCMV6-TTC7A-WT-FLAG, a higher expression of FLAG-tagged TTC7A and endogenous PI4KIIIa of about 80% each were detected in HEK293T cells, compared to C2BBe TTC7A-KO cells. HEK293T cells provided a reproducible and robust assay for protein analysis and prompting us to continue using them for the following protein experiments.

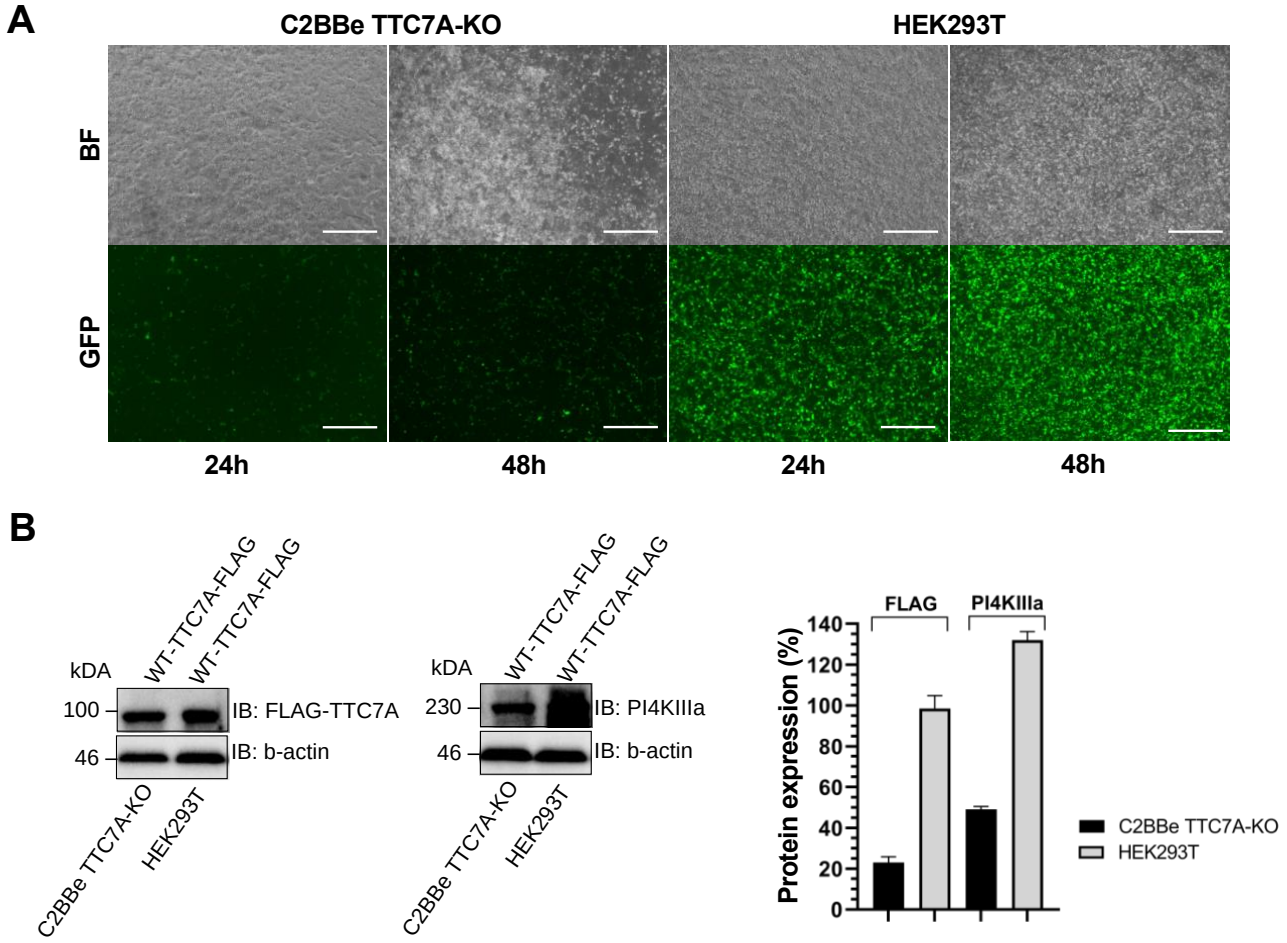

Figure 5. Transfection efficiency comparison between HEK239T and Caco2BBe TTC7A-KO cells.

(A) Caco2BBe (C2BBe) TTC7A-KO and HEK293T were transiently transfected with the pEGFP-C3 (GFP) contruct and were compared at (A) 24h and 48h. Bright field (BF) images were obtained with a stereomicroscope and the GFP images with a fluorescent filter (EVOS). Images were taken at 4x magnification and are representative, scale bars are 500 μm.

(B) Caco2BBe (C2BBe) TTC7A-KO and HEK293T were transiently transfected with the FLAG-tagged WT TTC7A construct and protein expression of (B) FLAG and PI4KIIIa were detected via immunoblotting. Images of blots are representative and were obtained with a ChemiDoc Imaging System. Protein expression was normalised to b-actin in ImageLab and GraphPad.

Missense TTC7A mutations did not affect TTC7A-PI4KIIIa binding

TTC7A missense gene products were co-immunoprecipitated with PI4KIIIa and non-precipitated lysates were used as input loading controls. To establish the efficacy of our coimmunoprecipitation assay, we initially tested the same mutations as in Avitzur et al A832T, E71K and used the truncating mutation Q526X as a negative control. In both A832T and E71K, PI4KIIIa and TTC7A-FLAG were detectable at expected values of ~230 kDA and ~100 kDA, respectively (Figure 6A). Furthermore, in Q526X, PI4KIIIa was not detected in the pulldown, and TTC7A-FLAG was faintly visible at ~60 kDA (Figure 6A, Pulldown). In the input two bands are visible in the PI4KIIIa lane, and in (Figure 6, Input) the immunoprecipitated only one PI4KIIIa band is present (Figure 6A, Pulldown). These results confirm that A832T and E71K mutations did not interrupt interaction with PI4KIIIa. After successful establishment of the immunoprecipitation assay, we confirmed six further mismatch TTC7A mutations (Figure 6A, bottom panels).

A832T, E71K and Q526X TTC7A variants did not inhibit PI4KIIIa kinase activity

To investigate the effect of mutations on PI4KIIIa's enzymatic activity, we performed a functional activity assay on PI4KIIIa precipitated with A832T, E71K or Q526X TTC7A variants, and measured the production of PI4P. Albeit the almost completely diminished PI4P, A832T and Q526X showed increased levels compared to E71K and WT TTC7A.

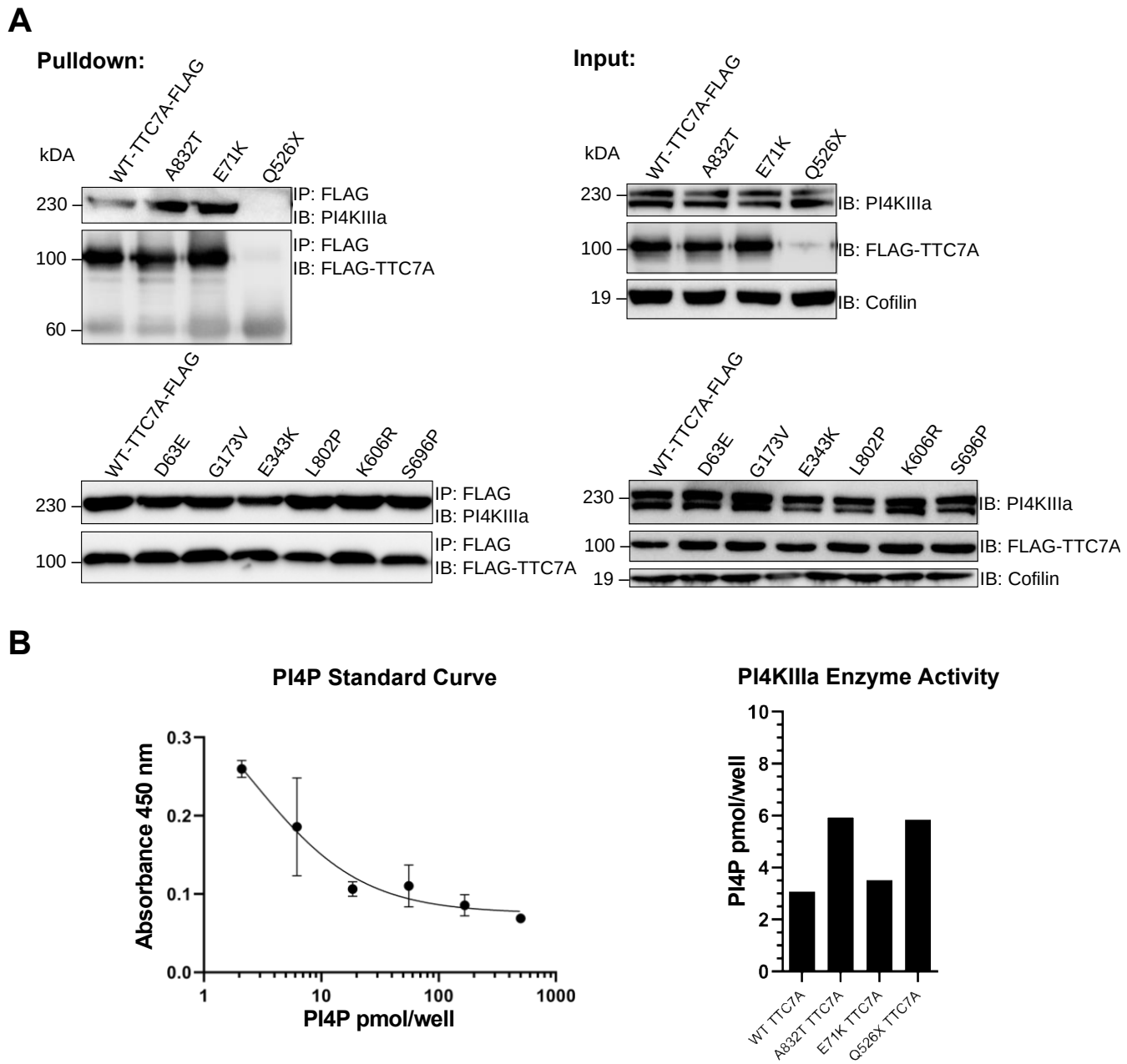

Figure 6. Coimmunoprecipitation of TTC7A and PI4KIIIa and quantification of PI4KIIIa activity.

(A) HEK293T cells were transiently transfected with FLAG-tagged WT TTC7A or mutant A832T, E71K, Q526X, D63E, G173V, E343K, L802P, K606R, S696P TTC7A constructs, whereby Q526X is coding for a premature stop codon and served as a negative control. Lysates were immunoprecipated with anti-FLAG antibody, and then immunoblotted using anti-PI4KIIIa and anti-FLAG antibodies. Non-FLAG-precipitated lysates were used as loading controls of the immunoprecipitation samples and were immunoblotted with anti-PI4KIIIa, anti-FLAG and anti-Cofilin antibodies. Pulldown represents immunoprecipitated TTC7A-PI4KIIIa and Input represents the control immunoblot.

(B) PI4KIIIa activity was measured via a competitive ELISA using triplicates of FLAG-immunoprecipitated lysates from transiently transfected HEK293T cells with FLAG-tagged WT or mutant A832T, E71KA, Q526X TTC7A. PI4P Standard Curve absorbance was measured at 450 nm in a microplate reader and the graph was generated using non-linear regression analysis (A log(agonist) vs. response – variable slope (four parameters) function in GraphPad. Values of samples were interpolated from the PI4P Standard Curve and correspond to PI4P production, indicator of PI4KIIIa activity in association with mutant TTC7A.

Discussion

In the case of inherited autosomal recessive diseases such as *TTC7A*, two deficient alleles are required for manifesting the disease. Therefore, the location and type of mutations within the *TTC7A* determine the severity of symptoms. TTC7A's involvement in numerous pathways active in intestinal homeostasis and immune system could explain the wide array of *TTC7A*-related symptoms. Challenged by the heterogenous disease progression of TTC7A-deficient genotypes, our goal was to unravel part of the underlying TTC7A pathway responsible for polarity defects in patient-derived

organoids. We established a reliable model system for assessing apicobasal polarity in patient-derived organoids from duodenum and successfully reversed polarisation defects using ROCK inhibitor. To further understand the phenotypical features of specific genotypes, we transiently expressed TTC7A mutant variants in C2BBe TTC7A-KO and HEK293T cell lines. All deficient *TTC7A* gene products were underexpressed with the exception of the S539L variant. We established that the mutated protein variants of TTC7A did not interrupt binding to its specific partner PI4KIIIa, which has not been previously reported. We also observed a diminished PI4KIIIa enzymatic activity, when complexed with mutated TTC7A.

We observed heterogeneous morphology (Figure 1), polarity (Figure 2) and maintenance requirements across all ileum-derived organoids including controls and patient, and not among duodenum-derived lines, suggesting that the origin of biopsies might have an effect on organoid behaviour. The observed differences between ileal and duodenal lines likely reflect the heterogenous environment of the human intestines. Different *TTC7A* gene variants might have variable manifestations along the digestive epithelium. That is why it is important to study samples obtained from different intestinal locations of the same patient. Control lines ile 2 and ile 3 presented with more polarity defects and difficulties maintaining during standard culture regiment, compared to P1 (Figure 2B). These structural and polarisation instabilities in the controls cannot be explained by *TTC7A*-deficiency. The observed phenotypes (Figure 1A, Ileum) could be produced by other genes, that are not known, or the ileum could be a more vulnerable tissue susceptible to environmental changes, compared to the duodenum. For these reasons, ileal samples were excluded from the study. In contrast, duodenal-derived organoids were considerably more stable and synchronised during both standard culturing and experiments (Figure 1B, Duodenum), creating a reproducible assay for polarity disease modelling. From all experiments performed with duodenal organoids, we calculated that ~80% is the baseline for normal polarity among healthy controls (Figure 2B, Duodenum). The remaining 20% consisted of 1/3 aberrant and 2/3 inverted organoids (Figure 2B, Duodenum). We hypothesise that mechanical dissociation is likely to produce polarisation defects in ~20% in the unaffected healthy organoids, which we considered as normal.

Although morphologically similar, P2 (duo) had more inverted and aberrant organoids than its controls, by ~10% for each group (Figure 2B). This is in agreement with previous findings that *TTC7A* mutations can generate epithelial polarisation defects [23,30,45,53]. Based on previous reports, we applied Y-27632 ROCK inhibitor and Leflunomide to correct polarity and morphological aberrations in *TTC7A*-deficient duodenum organoids [23,45]. Initially we observed a clear trend that with Y-27632 treatment, patient organoids reached normal polarity numbers, and with Leflunomide they did not (Figure 3A). It is evident that the increase in normality in P2 treated with ROCK inhibitor, is due to a decrease in inverted polarity and not in aberrant lumina. Similarly, Leflunomide and in combination with Y-27632, did not improve aberrant multiple lumen formation. The combination of Y-27632 and Leflunomide increased normal polarisation by correcting inverted polarity, similar to the Y-27632 treatment alone, suggesting that the correcting effects are produced by the ROCK inhibitor, and not by Leflunomide (Figure 3A). We confirmed these results in the following experiments, whereby the pharmacological inhibition of ROCK rescued the inverted phenotype of P2 and significantly improved overall morphology of duodenum-derived organoids (Figure 3B and C). Jardine et al identified Leflunomide as a potent inhibitor of the apoptotic cascade via caspase 3/7 in TTC7A KO cells and *ttc7a*$^{-/-}$ zebrafish [45]. Furthermore, Leflunomide-treated patient-derived colonoids with confirmed biallelic TTC7A mutations E71K, L304R, exhibited a higher survival rate and formed fewer multiple lumina [45]. In contrast, we did not observe the same effect of Leflunomide on multiple lumina formation or other polarity aberrancies. Although we did not investigate survival or apoptosis, no improvements (e.g. less aggregations or increase in organoid numbers) were observed in Leflunomide-treated samples. Fully inactive *TTC7A* is likely to cause a higher rate of apoptosis and therefore a more severe disease phenotype where Leflunomide can be effective, compared to biallelic *TTC7A* mutations that could lead to structural instabilities, and not necessarily to cell death. We did not identify Leflunomide useful for correcting polarisation, however, it could be investigated as an inhibitor of apoptosis in *TTC7A* mutations predicted to cause/lead to programmed cell death or in patients diagnosed with e.g. apoptotic enterocolitis. It is important to note that our drug assay is limited by short treatment intervals that might not be sufficient to produce phenotypical effects. Therefore, it could be useful to validate observed findings, if any, with RNA sequencing and quantitative PCR that can reveal subtle changes on the level of gene transcription. Then the obtained genetic data can inform on the design of future experiments to best address the heterogeneity of *TTC7A* deficiencies. For example, if Leflunomide is known to target some parts of the apoptotic cascade, cell survival or apoptotic assays investigating the presumed affected pathway components, are suitable for examining the drug efficacy in *TTC7A* deficiencies.

We showed that the addition of Y-27632 not only corrected polarisation defects, but also generated significantly more normal cystic organoids in both the duodenum control and patient lines (Figure 3B and C). This finding suggests that Y-27632 decreases duodenal organoid collapse and cell aggregations, that have been confirmed signatures of apoptosis [23]. Similar to our results, ROCK inhibitor decreased cell aggregation and improved morphology [23]. This makes sense, as Y-27632 is a potent inhibitor of cell death by dissociation (anoikis) and has been extensively used in cell culture regiments [50,54–60].

Given its known applications in cell culture, we believe that Y-27632 prevents single or detached cells to apoptose in mechanically dissociated organoids, regardless of *TTC7A*. However, Jardine et al demonstrated that cells knocked out of *TTC7A* showed phenotypes consistent with apoptosis including cytoskeletal disorganisation and overexpressed activated proapoptotic caspase 3. These effects were reversed by the inhibition of ROCK, implicating directly and specifically TTC7A in the Rho pathway [45]. Although we did not observe any morphological differences between C2BBe WT and TTC7A-KO cells (Figure 4A), the KO cells required less frequent passaging indicative of proliferative retardation, likely due to inactive TTC7A. Furthermore, there is a large body of evidence that solidifies the function of Rho effectors (e.g. ROCK) in the intestinal epithelial barrier and cell extrusion [47,49,61–65]. Apart from the epithelium, Rho signalling plays a primary functional role in immunity, T-cell development in the thymus and T cell migration [66,67]. This activity of Rho complements *TTC7A* deficiencies known to manifest primarily in the intestinal epithelium, thymus, and immune B/T cells. These novel findings further associate TTC7A with Rho in the pathogenesis of *TTC7A*-disease phenotypes such as IBD and CID [23,24,26,68].

Based on this evidence, we propose a possible mechanistic relationship between TTC7A and ROCK: malfunctional TTC7A leads to cytoskeletal disorganisation and ectopic protein expression in the intestinal epithelium and/or in immune cells, leading to aberrant polarisation and interrupted cell-cell contact. This in turn generates stress-related molecules and induces inflammation, activating Rho signalling. ROCK being a known substrate for apoptotic proteases granzyme B and caspase 3/7, can be constitutively activated as a consequence of TTC7A inactivity, leading to larger epithelial barrier disruptions and membrane blebbing, eventually resulting in cell death [69–71]. By blocking the activity of ROCK, cytoskeletal rearrangements and apoptosis caused by mechanical dissociation or deficient TTC7A, can be avoided. To address the missing gaps in the proposed mechanism, a series of conditional knockdowns (e.g. short hairpin RNA) targeting different *TTC7A* regions in epithelial cells with and without ROCK inhibitor, followed by immunostaining and immunoblotting, could reveal the domains responsible for polarity in relation to Rho signalling. To validate these findings, the Rho pathway can be targeted to reproduce *TTC7A*-deficient phenotypes. As it has overlapping functions with *TTC7A*, *TTC7B* should be knocked out to exclude redundant effects.

Many IBD patients including our samples P1 and P2, carry compound heterozygous mutations within the *TTC7A* [19]. To understand the individual effects of mutations, we generated a library of mismatch *TTC7A* variants (Table 1) and transiently expressed them in C2BBe TTC7A-KO cells. Immunoblotting revealed that all mutant versions of TTC7A were downregulated except for S539L (Figure 4C). Patient carrying S539L TTC7A variant was diagnosed with Type 1 atresia, facial dysmorphia, dental anomalities and inflammation, abnormalities that might be induced by TTC7A hyperactivity [32]. Mutations p. S696P and K606R, both present in P1 (ile), caused a ~70% decrease in TTC7A protein expression. Downregulation of both TTC7A-expressing alleles might explain the collapsed morphology of P1, where no clear lumen could be observed. P1 also carries a deficient *TTC7B* (unpublished data), which is known to have overlapping functions with *TTC7A* [4]. However, when mutated, TTC7B might not be able to rescue the decreased expression of TTC7A. Both TTC7 paralogues being affected is likely to result in a more severe disease phenotype, with structural defects observed in P1 (Figure 1A). Patient 2 carries G173V and L452P variants of TTC7A, which we linked to ectopic expression of F-actin and a6-integrin resulting in inverted polarisation (Figure 2B). Transient expression of G173V revealed a downregulation of its gene product by nearly half (Figure 4C), suggesting that G173V substitution might be partially responsible for the inverted phenotype, that is further exacerbated by the presence of L452P. ROCK inhibitor corrected inversion defects in P2 (Figure 3), suggesting that Y-27632 could be effective in patients carrying G173V and L452P TTC7A substitutions. TTC7A variants D63E, E75K, E343K, L802P, L399P, E71K and A832T TTC7A resulted in a variable decrease of TTC7A protein levels (Figure 4C), that might correspond to heterogenous disease manifestation in patients [23–25,28,30,33].

To inform us on the functionality of these various *TTC7A* mutants, we tested their ability to bind PI4KIIIa via immunoprecipitation. Following Avitzur et al's work, we adapted the immunoprecipitation protocol and initially tested the same mutations

A832T, E71K and Q526X. Similar to Avitzur et al, variants A832T and E71K were pulled with PI4KIIIa, and Q526X was not (Figure 6A), which confirmed the reliability of the immunoprecipitation assay. Q526X substitution is coding for a premature stop codon that leads to a nonsense-mediated *TTC7A* mRNA decay and therefore the protein is not produced and cannot bind PI4KIIIa. Avitzur et al detected a 63 kDa FLAG-TTC7A product in their immunoprecipitated Q526X sample, but we did not observe a clear band at that molecular weight (Figure 6A). Previously unreported, we were the first to confirm that D63E, G173V, E343K, L802P, K606R and S696P TTC7A variants were able to precipitate with PI4KIIIa, proving direct interaction between TTC7A and PI4KIIIa. Interestingly, in the input, there are two products present between 220 and 240 kDa immunoblotted with PI4KIIIa, and only one product in the immunoprecipitated blot. This finding suggests only one of the two PI4KIIIa products binds specifically to TTC7A. The input blot, where TTC7A is lacking (Q526X lane), also shows a fainter signal of the upper PI4KIIIa lane, indicating that the absence of TTC7A specifically reduced the expression of the upper 230 kDA corresponding to the full length PI4KIIIa protein. However, this does not explain the presence of two PI4KIIIa products. From literature we know there are other isoforms of PI4KIIIa, however, their sizes do not correspond to 220 kDA [72,73]. We also excluded the effect of transfection, as the appearance of multiple PI4KIIIa bands was observed in lysates of non-transfected HEK293T. A genetic and functional study of PI4KIIIa demonstrated that it is located on the 22q11.2 locus, a region known for its genetic instability, and that cancer cell lines, such as HEK293T, often have multiple copies of the PI4KIIIa transcript [74]. Therefore, it is possible that the two bands in our samples correspond to PI4KIIIa splice variants (e.g. wild type and mutated) of different lengths that could also require different post-translational modifications, producing proteins with slightly differing molecular weights. Our study of PI4KIIIa is limited by the oncogenic origin of HEK293T cells, and we suggest the use of a model system that is not associated with cancer.

We demonstrated that mutated TTC7A proteins are able to interact with PI4KIIIa, but albeit being bound to PI4KIIIa, deficient TTC7A can decrease PI4KIIIa enzymatic activity evident by decreased levels and ectopic distribution of PI4P [12,28,75]. Values from a single PI4KIIIa functional assay showed almost diminished levels of PI4P whereby A832T and Q526X variants resulted in higher PI4P concentrations, compared to E71K and WT TTC7A. A832T and E71K are predicted to be highly deleterious and to have reduced binding to PI4KIIIa resulting in a lower production of PI4P [19,28]. Q526X variant lacks TTC7A protein and therefore is expected to produce the least amount of PI4P. Our results were not comparable to previous findings and the obtained values were much lower than the referent values provided by the manufacturer, thus should be interpreted with caution. We propose future investigation of kinase activity to be carried out with established methods such as radiolabelled ATP tracing. Although, other kinases also produce PI4P, it has been demonstrated that PI4KIIIa is essential for the correct distribution of PI4P, whereby the cycling of PI4KIIIa to the plasma membrane is highly dependent on TTC7A and its interactions with the PI4KIIIa complex [12,15,16,76]. Therefore, it is important to study not only the levels but also the localisation of PI4P in relation to PI4KIIIa and deficient *TTC7A* variants. Since this has been demonstrated in cells, the next step is to validate these findings in a more comparable model such as the intestinal organoid. Locating and quantifying PI4KIIIa and PI4P in patient-derived organoids will help address the heterogenous polarisation defects in *TTC7A*-affected patients.

Conclusion

Using intestinal organoids, we established a robust assay for characterising polarity defects in *TTC7A*-deficient patients and identified a drug candidate to rescue the inverted apicobasal epithelial phenotype. Albeit lacking the complexity of a whole organism, patient-derived organoids express the features of the organ they originated from, and moreover, carry patient-specific signatures. Our model system can be further used to test epithelial barrier function using derivatives of the transwell assay, and bacterial stimulations mimicking pathogenic invasions. The organoid is also amendable to genetic manipulation that can further elucidate the effects of individual *TTC7A* mutations, to help unravel heterogeneity among disease phenotypes. The 3D nature of the organoid system allows the spatiotemporal investigation of protein (co-)localisation and cytoskeletal elements utilising techniques like immunohistochemistry and live imaging. These features of the intestinal organoid make it a powerful tool for IBD disease modelling, experimental drug screening and the development of personalised treatment plans. To realise the full extent of the TTC7A interactome, efforts should be focused on meticulously targeting the other members of the PI4KIIIa complex and their isoforms, as well as the Rho pathway. This knowledge will help elucidate specific roles of TTC7A in health and disease. When sufficient robust data has been generated, such as our duodenum apicobasal polarity data, it can be processed with a bioinformatic tool to produce an algorithm for *TTC7A* that will help design suitable assays and predict the most appropriate care for patients, opening another door of many possibilities.

Acknowledgements

We thank Jerold Turner for the Caco2BBe epithelial cell line and Boston's Children Hospital and University Medical Centre Utrecht for the intestinal biopsies, and the Hubrecht Institute for the preparation of buffers and bacterial media. On a personal note, I would like to thank Edward Nieuwenhuis and Michal Mokry for their helpful feedback and having trust in my ideas throughout my scientific journey. Special thanks to Maaike de Vries, Emilia Nagyova and Zahra Shojaeijeshvaghani for the practical, theoretical, and emotional support, as well as, to the rest of the Pediatric Gastroenterology members.

References

1. https://www.proteinatlas.org/ENSG00000068724-TTC7A/tissue. Tissue expression of TTC7A - summary - The Human Protein Atlas.
2. Blatch, G. L. & Lässle, M. The tetratricopeptide repeat: a structural motif mediating protein-protein interactions. *BioEssays* **21**, 932–939 (1999).
3. Zeytuni, N. & Zarivach, R. Structural and Functional Discussion of the Tetra-Trico-Peptide Repeat, a Protein Interaction Module. *Structure* **20**, 397–405 (2012).
4. http://useast.ensembl.org/Homo_sapiens/Gene/Compara_Paralog?db=core. Gene: TTC7A (ENSG00000068724) - paralogues - Homo sapiens - Ensembl genome browser 92.
5. Lees, J. A. *et al.* Architecture of the human PI4KIIIα lipid kinase complex. *Proceedings of the National Academy of Sciences* **114**, 13720–13725 (2017).
6. Baskin, J. M. *et al.* The leukodystrophy protein FAM126A (hyccin) regulates PtdIns(4)P synthesis at the plasma membrane. *Nature Cell Biology* **18**, 132–138 (2016).
7. Chung, J., Nakatsu, F., Baskin, J. M. & de Camilli, P. Plasticity of PI4KIIIα interactions at the plasma membrane. *EMBO reports* **16**, 312–320 (2015).
8. Lees, J. A. *et al.* Architecture of the human PI4KIIIα lipid kinase complex. *Proceedings of the National Academy of Sciences* **114**, 13720–13725 (2017).
9. Baskin, J. M. *et al.* The leukodystrophy protein FAM126A (hyccin) regulates PtdIns(4)P synthesis at the plasma membrane. *Nature Cell Biology* **18**, 132–138 (2016).
10. di Paolo, G. & de Camilli, P. Phosphoinositides in cell regulation and membrane dynamics. *Nature* **443**, 651–657 (2006).
11. Balla, T. Phosphoinositides: Tiny Lipids With Giant Impact on Cell Regulation. *Physiological Reviews* **93**, 1019–1137 (2013).
12. Nakatsu, F. *et al.* PtdIns4P synthesis by PI4KIIIα at the plasma membrane and its impact on plasma membrane identity. *Journal of Cell Biology* **199**, 1003–1016 (2012).
13. D'Angelo, G., Vicinanza, M., di Campli, A. & de Matteis, M. A. The multiple roles of PtdIns(4) *P* – not just the precursor of PtdIns(4,5) *P* 2. *Journal of Cell Science* **121**, 1955–1963 (2008).
14. Balla, A., Tuymetova, G., Tsiomenko, A., Várnai, P. & Balla, T. A Plasma Membrane Pool of Phosphatidylinositol 4-Phosphate Is Generated by Phosphatidylinositol 4-Kinase Type-III Alpha: Studies with the PH Domains of the Oxysterol Binding Protein and FAPP1. *Molecular Biology of the Cell* **16**, 1282–1295 (2005).
15. Zhai, C. *et al.* Ypp1/YGR198w plays an essential role in phosphoinositide signalling at the plasma membrane. *Biochemical Journal* **415**, 455–466 (2008).
16. Baird, D., Stefan, C., Audhya, A., Weys, S. & Emr, S. D. Assembly of the PtdIns 4-kinase Stt4 complex at the plasma membrane requires Ypp1 and Efr3. *Journal of Cell Biology* **183**, 1061–1074 (2008).
17. Vaillancourt, F. H. *et al.* Evaluation of Phosphatidylinositol-4-Kinase III as a Hepatitis C Virus Drug Target. *Journal of Virology* **86**, 11595–11607 (2012).
18. Thakur, P. C., Davison, J. M., Stuckenholz, C., Lu, L. & Bahary, N. Dysregulated phosphatidylinositol signaling promotes

endoplasmic-reticulum-stress-mediated intestinal mucosal injury and inflammation in zebrafish. *Disease Models & Mechanisms* (2013) doi:10.1242/dmm.012864.
19. Jardine, S., Dhingani, N. & Muise, A. M. TTC7A: Steward of Intestinal Health. *Cellular and Molecular Gastroenterology and Hepatology* **7**, 555–570 (2019).
20. Jardine, S., Dhingani, N. & Muise, A. M. TTC7A: Steward of Intestinal Health. *CMGH* vol. 7 (2019).
21. El-Daher, M.-T. *et al.* Tetratricopeptide repeat domain 7A is a nuclear factor that modulates transcription and chromatin structure. *Cell Discovery* **4**, 61 (2018).
22. Agarwal, N. S. *et al.* Tetratricopeptide Repeat Domain 7A (TTC7A) Mutation in a Newborn with Multiple Intestinal Atresia and Combined Immunodeficiency. *Journal of Clinical Immunology* **34**, 607–610 (2014).
23. Bigorgne, A. E. *et al.* TTC7A mutations disrupt intestinal epithelial apicobasal polarity. *Journal of Clinical Investigation* **124**, 328–337 (2014).
24. Chen, R. *et al.* Whole-exome sequencing identifies tetratricopeptide repeat domain 7A (TTC7A) mutations for combined immunodeficiency with intestinal atresias. *Journal of Allergy and Clinical Immunology* **132**, 656-664.e17 (2013).
25. Lien, R. *et al.* Novel Mutations of the Tetratricopeptide Repeat Domain 7A Gene and Phenotype/Genotype Comparison. *Frontiers in Immunology* **8**, (2017).
26. Samuels, M. E. *et al.* Exome sequencing identifies mutations in the gene *TTC7A* in French-Canadian cases with hereditary multiple intestinal atresia. *Journal of Medical Genetics* **50**, 324–329 (2013).
27. https://genecards.weizmann.ac.il/v3/cgi-bin/carddisp.pl?gene=TTC7A&lm_expand=all&search=ttc7a#lifemap_expression. TTC7A expression in embryonic tissues and stem cells.
28. Avitzur, Y. *et al.* Mutations in Tetratricopeptide Repeat Domain 7A Result in a Severe Form of Very Early Onset Inflammatory Bowel Disease. *Gastroenterology* **146**, 1028–1039 (2014).
29. Bigorgne, A. E. *et al.* TTC7A mutations disrupt intestinal epithelial apicobasal polarity. *Journal of Clinical Investigation* **124**, 328–337 (2014).
30. Lemoine, R. *et al.* Immune deficiency–related enteropathy-lymphocytopenia-alopecia syndrome results from tetratricopeptide repeat domain 7A deficiency. *Journal of Allergy and Clinical Immunology* **134**, 1354-1364.e6 (2014).
31. Kammermeier, J. *et al.* Stem cell transplantation for tetratricopeptide repeat domain 7A deficiency: long-term follow-up. *Blood* **128**, 1306–1308 (2016).
32. Neves, J. F. *et al.* Missense mutation of TTC7A mimicking tricho-hepato-enteric (SD/THE) syndrome in a patient with very-early onset inflammatory bowel disease. *European Journal of Medical Genetics* **61**, 185–188 (2018).
33. Fayard, J. *et al.* TTC7A mutation must be considered in patients with repeated intestinal atresia associated with early inflammatory bowel disease: Two new case reports and a literature review. *Archives de Pédiatrie* **25**, 334–339 (2018).
34. Fullerton, B. S., Velazco, C. S., Hong, C. R., Carey, A. N. & Jaksic, T. High Rates of Positive Severe Combined Immunodeficiency Screening Among Newborns with Severe Intestinal Failure. *JPEN. Journal of parenteral and enteral nutrition* **42**, 239–246 (2018).
35. Mandiá, N. *et al.* Congenital intestinal atresias with multiple episodes of sepsis. *Medicine* **97**, e10939 (2018).
36. Yang, W. *et al.* Compound heterozygous mutations in TTC7A cause familial multiple intestinal atresias and severe combined immunodeficiency. *Clinical Genetics* **88**, 542–549 (2015).
37. Woutsas, S. *et al.* Hypomorphic mutation in TTC7A causes combined immunodeficiency with mild structural intestinal defects. *Blood* **125**, 1674–1676 (2015).
38. Guanà, R. *et al.* The Complex Surgical Management of the First Case of Severe Combined Immunodeficiency and Multiple Intestinal Atresias Surviving after the Fourth Year of Life. *Pediatric*

Gastroenterology, Hepatology & Nutrition **17**, 257 (2014).
39. Lawless, D. *et al.* Bialellic Mutations in Tetratricopeptide Repeat Domain 7A (TTC7A) Cause Common Variable Immunodeficiency-Like Phenotype with Enteropathy. *Journal of Clinical Immunology* **37**, 617–622 (2017).
40. Kammermeier, J. *et al.* Stem cell transplantation for tetratricopeptide repeat domain 7A deficiency: long-term follow-up. *Blood* **128**, 1306–1308 (2016).
41. Thiagarajah, J. R. *et al.* Advances in Evaluation of Chronic Diarrhea in Infants. *Gastroenterology* **154**, 2045-2059.e6 (2018).
42. Gilroy, R. K. *et al.* Donor immune reconstitution after liver–small bowel transplantation for multiple intestinal atresia with immunodeficiency. *Blood* **103**, 1171–1174 (2004).
43. Medical Advisory Secretariat. Small bowel transplant: an evidence-based analysis. *Ontario health technology assessment series* **3**, 1–72 (2003).
44. Lien, R. *et al.* Novel Mutations of the Tetratricopeptide Repeat Domain 7A Gene and Phenotype/Genotype Comparison. *Frontiers in Immunology* **8**, (2017).
45. Jardine, S. *et al.* Drug Screen Identifies Leflunomide for Treatment of Inflammatory Bowel Disease Caused by TTC7A Deficiency. *Gastroenterology* **158**, 1000–1015 (2020).
46. O'Brien, L. E., Zegers, M. M. P. & Mostov, K. E. Building epithelial architecture: insights from three-dimensional culture models. *Nature Reviews Molecular Cell Biology* **3**, 531–537 (2002).
47. Yu, W. *et al.* Involvement of RhoA, ROCK I and myosin II in inverted orientation of epithelial polarity. *EMBO reports* **9**, 923–929 (2008).
48. Bigorgne, A. E. *et al.* TTC7A mutations disrupt intestinal epithelial apicobasal polarity. *Journal of Clinical Investigation* **124**, 328–337 (2014).
49. Reed, R. A. *et al.* Morphogenesis of the primitive gut tube is generated by Rho/ROCK/myosin IIâ€“mediated endoderm rearrangements. *Developmental Dynamics* **238**, 3111–3125 (2009).
50. Sato, T. *et al.* Long-term Expansion of Epithelial Organoids From Human Colon, Adenoma, Adenocarcinoma, and Barrett's Epithelium. *Gastroenterology* **141**, 1762–1772 (2011).
51. Pleguezuelos-Manzano, C. *et al.* Establishment and Culture of Human Intestinal Organoids Derived from Adult Stem Cells. *Current Protocols in Immunology* **130**, (2020).
52. Sato, T. *et al.* Single Lgr5 stem cells build crypt-villus structures in vitro without a mesenchymal niche. *Nature* **459**, 262–265 (2009).
53. Helms, C. *et al.* The Tetratricopeptide Repeat Domain 7 Gene is Mutated in Flaky Skin Mice: A Model for Psoriasis, Autoimmunity, and Anemia. *Experimental Biology and Medicine* **230**, 659–667 (2005).
54. Claassen, D. A., Desler, M. M. & Rizzino, A. ROCK inhibition enhances the recovery and growth of cryopreserved human embryonic stem cells and human induced pluripotent stem cells. *Molecular Reproduction and Development* **76**, 722–732 (2009).
55. Watanabe, K. *et al.* A ROCK inhibitor permits survival of dissociated human embryonic stem cells. *Nature Biotechnology* **25**, 681–686 (2007).
56. Martin-Ibanez, R. *et al.* Novel cryopreservation method for dissociated human embryonic stem cells in the presence of a ROCK inhibitor. *Human Reproduction* **23**, 2744–2754 (2008).
57. Li, X., Meng, G., Krawetz, R., Liu, S. & Rancourt, D. E. The ROCK Inhibitor Y-27632 Enhances the Survival Rate of Human Embryonic Stem Cells Following Cryopreservation. *Stem Cells and Development* **17**, 1079–1086 (2008).
58. Li, X., Krawetz, R., Liu, S., Meng, G. & Rancourt, D. E. ROCK inhibitor improves survival of cryopreserved serum/feeder-free single human embryonic stem cells. *Human Reproduction* **24**, 580–589 (2008).
59. Heng, B. C. Effect of Rho-associated kinase (ROCK) inhibitor Y-27632 on the post-thaw viability of cryopreserved human bone

marrow-derived mesenchymal stem cells. *Tissue and Cell* **41**, 376–380 (2009).
60. Riento, K. & Ridley, A. J. ROCKs: multifunctional kinases in cell behaviour. *Nature Reviews Molecular Cell Biology* **4**, 446–456 (2003).
61. Eisenhoffer, G. T. *et al.* Crowding induces live cell extrusion to maintain homeostatic cell numbers in epithelia. *Nature* **484**, 546–549 (2012).
62. Mack, N. A. & Georgiou, M. The interdependence of the Rho GTPases and apicobasal cell polarity. *Small GTPases* **5**, e973768 (2014).
63. Slattum, G., McGee, K. M. & Rosenblatt, J. P115 RhoGEF and microtubules decide the direction apoptotic cells extrude from an epithelium. *Journal of Cell Biology* **186**, 693–702 (2009).
64. Schlegel, N., Meir, M., Spindler, V., Germer, C.-T. & Waschke, J. Differential role of Rho GTPases in intestinal epithelial barrier regulation in vitro. *Journal of Cellular Physiology* **226**, 1196–1203 (2011).
65. Terry, S., Nie, M., Matter, K. & Balda, M. S. Rho Signaling and Tight Junction Functions. *Physiology* **25**, 16–26 (2010).
66. Saoudi, A., Kassem, S., Dejean, A. S. & Gaud, G. Rho-GTPases as key regulators of T lymphocyte biology. *Small GTPases* **5**, e983862 (2014).
67. Bros, Haas, Moll & Grabbe. RhoA as a Key Regulator of Innate and Adaptive Immunity. *Cells* **8**, 733 (2019).
68. Moreno, L. A. *et al.* Severe combined immunodeficiency syndrome associated with autosomal recessive familial multiple gastrointestinal atresias: Study of a family. *American Journal of Medical Genetics* **37**, 143–146 (1990).
69. Coleman, M. L. *et al.* Membrane blebbing during apoptosis results from caspase-mediated activation of ROCK I. *Nature Cell Biology* **3**, 339–345 (2001).
70. Hopkins, A. M., Walsh, S. v., Verkade, P., Boquet, P. & Nusrat, A. Constitutive activation of Rho proteins by CNF-1 influences tight junction structure and epithelial barrier function. *Journal of Cell Science* **116**, 725–742 (2003).
71. Ehrenschwender, M. *et al.* Mutant PIK3CA licenses TRAIL and CD95L to induce non-apoptotic caspase-8-mediated ROCK activation. *Cell Death & Differentiation* **17**, 1435–1447 (2010).
72. Nakagawa, T., Goto, K. & Kondo, H. Cloning, Expression, and Localization of 230-kDa Phosphatidylinositol 4-Kinase. *Journal of Biological Chemistry* **271**, 12088–12094 (1996).
73. Balla, T. *et al.* Isolation and Molecular Cloning of Wortmannin-sensitive Bovine Type III Phosphatidylinositol 4-Kinases. *Journal of Biological Chemistry* **272**, 18358–18366 (1997).
74. Szentpetery, Z., Szakacs, G., Bojjireddy, N., Tai, A. W. & Balla, T. Genetic and functional studies of phosphatidyl-inositol 4-kinase type IIIα. *Biochimica et Biophysica Acta (BBA) - Molecular and Cell Biology of Lipids* **1811**, 476–483 (2011).
75. Bojjireddy, N. *et al.* Pharmacological and Genetic Targeting of the PI4KA Enzyme Reveals Its Important Role in Maintaining Plasma Membrane Phosphatidylinositol 4-Phosphate and Phosphatidylinositol 4,5-Bisphosphate Levels. *Journal of Biological Chemistry* **289**, 6120–6132 (2014).
76. Balla, A. & Balla, T. Phosphatidylinositol 4-kinases: old enzymes with emerging functions. *Trends in Cell Biology* **16**, 351–361 (2006).